International Journal of Hydrogen Energy 80 (2024) 280–288

Contents lists available at ScienceDirect

International Journal of Hydrogen Energy

journal homepage: www.elsevier.com/locate/he

In-plane heterostructures of transition metal dichalcogenide monolayers with enhanced charge separation and effective overall water splitting

Shafiq Ur Rehman [a,*], Qihui Sun [a,b], Junwei Wang [a], Weiqiang Lv [a,b], Azim Khan [a], Yifan Liu [a], Nasir Mahmood [c,**], Jian Xian [a,b,***]

[a] Yangtze Delta Region Institute (Huzhou), University of Electronic Science and Technology of China, Huzhou, 313001, China
[b] School of Materials and Energy, University of Electronic Science and Technology of China, Chengdu, 611731, China
[c] School of Science, RMIT University, 124 La Trobe Street, 3001, Melbourne, Victoria, Australia

ARTICLE INFO

Handling Editor: Ramazan Solmaz

Keywords:
Photocatalytic water splitting
Charge separation
In-plane interface
STH efficiency
Molecular dynamic simulation
First-principles calculations

ABSTRACT

Finding a catalyst for overall water splitting (OWS) with robust thermodynamic stability and optimal electronic characteristics remains a significant challenge. This study investigates the thermodynamic stability and interfacial properties of zigzag and armchair MoS_2/WS_2 in-plane heterostructures using ab-initio molecular dynamics (AIMD) and density functional theory (DFT) simulations. The motivation behind this research is to identify highly efficient and stable catalysts for OWS. The AIMD simulations confirm the thermodynamic stability of both heterostructures under working conditions. Notably, the zigzag MoS_2/WS_2 in-plane heterostructure demonstrates superior charge separation efficiency, with larger conduction band (0.91 eV) and valence band (0.71 eV) offsets compared to the armchair configuration. The unique chemical bonding and type-II band alignment at the zigzag junction enhance charge transfer, resulting in excellent catalytic activities with ultralow overpotentials for oxygen (0.96 V) and hydrogen (0.3 V) evolution reactions at pH = 0. Additionally, the zigzag heterostructure achieves a high solar-to-hydrogen (STH) conversion efficiency of 12.29%, making it a promising candidate for practical applications in OWS. These findings contribute to the advancement of water splitting technology and encourage further research on in-plane interface formation among diverse materials.

1. Introduction

Photocatalysis is emerging as a pivotal green energy technology, leveraging solar illumination to facilitate the decomposition of organic pollutants, water splitting, CO_2 reduction, and other transformative processes. Nevertheless, the pervasive challenge impeding broad implementation lies in the scarcity of cost-effective and exceptionally efficient semiconductor photocatalytic materials [1–5]. Photocatalytic water splitting has been utilizing metal oxides, metal nitrides, metal sulfides, oxynitrides, and oxysulphides for photocatalytic H_2 evolution [6–8]. But theses catalysts suffered from serious issues, such as large band gap ($E_g > 3$ eV), low hydrogen conversion efficiencies, high charge recombination rate, photo-corrosion and low quantum yield (<10%) [9,10]. 2D semiconductors recently have attracted great attention as an alternative in water splitting, due to their proper band gaps, large surface area, high optical absorption, and excellent thermal and chemical stability [11–17]. Among them, TMDCs (transition metal dichalcogenides), such as WS_2, $MoSe_2$, WSe_2, MoS_2 and $MoTe_2$ are particularly suitable for visible-light-driven photocatalysis [11,18–20]. However, water splitting based on TMDCs suffers from a high rate of exciton recombination, because of the extremely large exciton binding energies in low-dimensional systems. Moreover, most TMDCs have shown low thermal stability and the defects in TMDCs undergo significant photo-corrosion [21]. It is well-known that the high rate of exciton recombination can be controlled in heterojunctions, exhibiting efficient charge separation [22–24]. So far, researchers have identified several types of heterojunctions aimed at boosting the efficacy of the photocatalysts [21–26]. Among them, direct Z-scheme heterojunctions and type-II heterojunctions are widely studied based on their mechanisms of charge separation [21,23–27]. The unique electronic band alignment in Z-scheme and type-II heterojunctions making them more attractive for photocatalytic water splitting [28–33]. Recently, heterostructures

* Corresponding author.
** Corresponding author.
*** Corresponding author. Yangtze Delta Region Institute (Huzhou), University of Electronic Science and Technology of China, Huzhou 313001, China.
E-mail addresses: shafiqphy123@gmail.com (S.U. Rehman), nasir.mahmood@rmit.edu.au (N. Mahmood), jianxian@uestc.edu.cn (J. Xian).

https://doi.org/10.1016/j.ijhydene.2024.07.171
Received 25 April 2024; Received in revised form 20 June 2024; Accepted 11 July 2024

formed by van der Waals (vdW) interactions gained great attention for photocatalysis application due to their conventional type-II band alignment [23,25,34–36]. Although the type-II heterojunction can ideally separate holes and electrons, these vdW heterostructures possess interlayer distances of 3-4Å, which physically leads to fast electron-hole recombination. The fast recombination process hindering their effective participation in the OER (oxygen evolution reaction) and HER (hydrogen evolution reaction).

To overcome the high exciton (electron-hole) recombination in vdW heterojunctions, in-plane TMDCs heterostructures has been widely investigated, which are formed laterally by covalent bonds [34–37]. In in-plane heterostructures of TMDCs, the bonding between the two materials occurs through chemical interactions. Unlike vertical heterostructures, where Coulomb interactions keep electrons and holes separated in opposite directions, in-plane heterostructures yield a more substantial in-plane dipole, predominantly constrained by layer separation [34,38]. In in-plane heterostructures, the spatial separation results in a reduced exciton binding energy compared to interlayer excitons [34,38]. Recently, few-layers WS_2–MoS_2 in-plane heterostructures have demonstrated excellent STH efficiency and photocatalytic activity for OWS [39]. Similarly, the SnO_2/CdS, C/C_3N_4 and MoS_2/MoC in-plane heterostructures enhances carrier separation and optimizes surface-hydrogen-desorption energy, resulting in superior photocatalytic hydrogen production [30,39–41]. Additionally, the AlP_3-GaP_3 in-plane heterostructure has shown good chemical stability, high STH efficiency (16%), and suitable band alignment for water splitting [42].

Herein, we used AIMD and DFT simulations to explore the thermodynamic stability, interface properties and catalytic potential of MoS_2/WS_2 in-plane heterostructure. We have combined the isolated monolayers MoS_2 and WS_2 through covalent bonding in a unit cell. At the lateral heterostructure, we observed two possibles configuration i. e zigzag and armchair. Each configuration shows the thermodynamically stability for water splitting, but the zigzag configuration was found with enrich electronic properties, large band offsets formation, and enhanced charge separation. We also explored a sort of variations in the interface interactions which influences these properties. Furthermore, the suitability of the in-plane heterostructure was studied for the OWS. In the zigzag configuration of MoS_2/WS_2, we observed rapid charge transfer and enhanced charge separation with large conduction and valence band offsets 0.91 eV and 0.71 eV respectively.

The zigzag MoS_2/WS_2 in-plane heterostructure exhibits excellent photocatalytic performance, with overpotentials of 0.96 V and 0.3 V for oxygen and hydrogen evolutions respectively, at pH = 0. It also achieves a 12.29% STH conversion efficiency, making it highly promising for hydrogen production. This outstanding efficiency is driven by effective charge separation, minimal exciton recombination, and low overpotentials, emphasizing its significance for sustainable energy applications. Our work is theoretical, it provides valuable insights that can guide experimental research and deepen our understanding of in-plane TMDC heterostructures. This framework can help inform future studies and experimental validations.

2. Computational detail

Advanced quantum computational chemistry methods were utilized in our study, employing DFT within the VASP (Vienna Abinitio Simulation Package) software. We employed the GGA-PBE (generalized gradient approximation) to consider electron-electron interactions in materials [43,44]. Furthermore, we conducted HSE06 calculations on a parallel supercomputer to ensure precise energy calculations for pristine materials and their in-plane heterostructures [45]. For the calculation of plan waves the cut-off energy was set to (400 eV) for MoS_2 and WS_2 monolayers and (450 eV) for zigzag and armchair MoS_2/WS_2 heterostructures. Structural relaxation for both monolayers and heterostructures was performed with a force criterion of (0.01 eVÅ^{-1}).

The (1s, 9d) orbitals were considered as highest occupied orbitals for Mo and W, while (2s, 4p) were treated as the highest occupied orbitals for S. To prevent self-interactions among unit cells, a 15 Å vacuum were kept in the c-axis. In the energy calculation with PBE and HSE06, the kpoints (9 × 9 × 1) was chosen. In case of PBE the mesh was refined to (18 × 18 × 1) and the HSE06 calculations was carried at the same kpoints [46]. The spin orbit coupling (SOC) effect was incorporated into the band structures calculations for the heavy transition metals (Mo, W). The vdW energy correction terms in the heterostructures were taken into account by incorporating the corrections model of Grimme (DFT-D3) to minimize the structures [46,47]. The AIMD simulations was carried out at temperatures 300K–373K with a time step of 10 ps. The selective dynamic approach was effectively utilized during the relaxation of 3 × 3 × 1 supercell of both zigzag and armchair MoS_2/WS_2 heterostructures. The key advantage of the selective dynamic approach is that, we can consider a large super cell for the adsorption of intermediates surrounding the heterojunction of zigzag in-plane heterostructure.

3. Results and discussion

3.1. The thermal stability and electronic properties

Initially, the electronic and structure properties of monolayers 2H–MoS_2 and 2H-WS_2 were investigated with PBE and HSE06 functionals, their relaxed lattice constants and band gaps calculated with two functionals are shown in Table 1. The monolayers analyzed in this study exhibit direct band gaps at the K-point, consistent with findings from prior research [48]. Lattice constants of monolayers MoS_2 and WS_2 have perfectly matched, which shows the suitability of the composite formation between the two layers. In constructing the MoS_2/WS_2 in-plane heterostructure, we used a rectangular unit cell of MoS_2 monolayer, as shown in Fig. 1(a). We have constructed two types of edges for in-plane heterostructure of MoS_2/WS_2 i.e. armchair (ac-MoS_2/WS_2) and zigzag (zz-MoS_2/WS_2), as given in Fig. 1(b and c). The energetic stabilities of zz-MoS_2/WS_2 and ac-MoS_2/WS_2 edges were determined by the edge energy calculations formula; $E_{edge} = \left(E_{with\ edge} - E_{without\ edge}\right)/2L$, where E_{edge}, $E_{with\ edge}$, $E_{without\ edge}$ and L represents the total edge energy per unit length (eV/Å), total energy with edge per unit cell, energy of the pristine monolayers in a unit cell and total length of the edge, respectively. The HSE06 calculated edge energies for ac-MoS_2/WS_2 and zz-MoS_2/WS_2 are −1.73 eV/Å and −2.61 eV/Å respectively. The negative sign shows that exothermic reaction occurs during the formation of edges and both edges are energetically favorable. The edge energy shows that the zz-MoS_2/WS_2 heterostructure are more stable energetically.

The calculated band gaps along the direction of junctions with GGA-PBE and HSE06 functionals for zz-MoS_2/WS_2 and ac-MoS_2/WS_2 in-plane interfaces are given in Fig. 2 (a-d), and the numerical values of the band

Table 1
The lattice constants (a), band gap (E_g) and edge energies of 2H–MoS_2 and 2H-WS_2 monolayers, zz-MoS_2/WS_2 and ac-MoS_2/WS_2 in-plan heterostructures calculated with PBE and HSE06 are shown in table below.

system	a (Å)	E_g (eV)	Edge energy (eV/Å)	CBM (eV)	VBM (eV)
GGA-PBE					
MoS_2	3.15	1.68	–	−2.9	−5.01
WS_2	3.16	1.75	–	−2.51	−5.1
zz-MoS_2/WS_2	3.17	2.16	−2.14	−3.21	−5.32
Ac-MoS_2/WS_2	3.17	1.71	−1.24	−2.98	−5.30
HSE06					
MoS_2	3.25	2.13	–	−3.99	−6.02
WS_2	3.24	2.73	–	−3.69	−5.72
zz-MoS_2/WS_2	3.18	2.27	−2.61	−3.64	−5.90
Ac-MoS_2/WS_2	3.18	2.28	−1.73	−3.60	−5.87

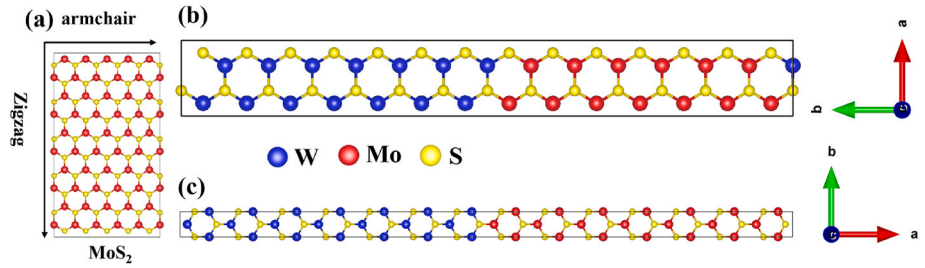

Fig. 1. Geometric structures of MoS_2/WS_2 in-plane heterostructure; (a) MoS_2 monolayer with zigzag and armchair directions, (b) armchair interface, (c) zigzag interface.

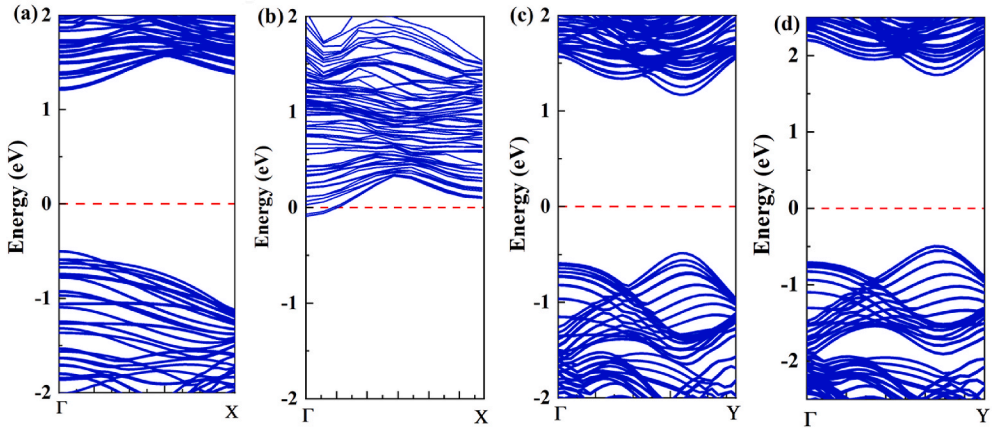

Fig. 2. Band structures calculated with PBE and HSE06 for; (a, b) armchair, (c, d) zigzag respectively. Where the red line indicates the fermi level. (For interpretation of the references to colour in this figure legend, the reader is referred to the Web version of this article.)

gaps are shown in Table 1. The band gap values obtained with GGA-PBE often exhibit underestimation. To address this, we employed the HSE06 functional to obtain more accurate band gap values. The HSE06 band gaps for zz-MoS_2/WS_2 and ac-MoS_2/WS_2 are 2.27 eV and 2.28 eV respectively. Both edges exhibit band gaps conducive to solar water splitting, rendering them viable visible-light photocatalysts [10]. For effective water splitting process, a crucial consideration is the alignment of energy edges of a photocatalyst with the standard redox potentials of water [10]. To address this, we calculated the CBM (conduction band edge) and VBM (valence band edge) relative to the vacuum level for zz-MoS_2/WS_2 and ac-MoS_2/WS_2. The results indicate that for zz-MoS_2/WS_2, the CBM and VBM are positioned at −3.64 eV and −5.90 eV, respectively. Similarly, for ac-MoS_2/WS_2, the CBM and VBM are positioned at −3.60 eV and −5.87 eV, respectively. The standard potentials values for the HER are −4.44 eV and for OER is −5.67 eV [5]. The energy edge positions of both heterostructures are straddling with the standard potentials of water. These findings underscore the potential suitability of both edges for effective visible-light photocatalysis in the context of overall water splitting. The energy edge positions were calculated with the electrostatic potential method. The zz-MoS_2/WS_2 and ac-MoS_2/WS_2 heterostructures exhibited suitable band gaps and energy edges positions for water splitting. Therefore, zz-MoS_2/WS_2 and ac-MoS_2/WS_2 in-plane interfaces can effectively utilizing the visible light to breakdown the water molecules into hydrogen and oxygen [10].

To verify the thermodynamic stability of the MoS_2 and WS_2 monolayers, as well as the zigzag (zz-MoS_2/WS_2) and armchair (ac-MoS_2/WS_2) in-plane interfaces, we conducted AIMD simulations in water at temperatures of 300 K and 373 K. These simulations were performed using a $3 \times 3 \times 1$ supercell with a time step of 1 fs and a total simulation duration of 10 ps. Throughout the AIMD simulations, both the monolayers and in-plane interfaces exhibited excellent thermodynamic stability in water. The structural geometries remained stable, and no significant fluctuations in bond lengths were observed for either the pristine monolayers or the heterostructures. Fig. 3 (a, b) & **(c, d)** shows different orientations of the simulated geometries of MoS_2 and WS_2 monolayers at various temperatures, respectively. Similarly, Fig. 3 (e, f) presents the geometries of zz-MoS_2/WS_2 and ac-MoS_2/WS_2 in-plane interfaces at the elevated temperature of 373 K. The results demonstrate that both the pristine monolayers and their in-plane interfaces maintain thermodynamic stability in water at both room temperature and higher temperature. The total energy fluctuations for the pristine monolayers, as well as the zz-MoS_2/WS_2 and ac-MoS_2/WS_2 in-plane interfaces, were negligible, further corroborating their excellent thermodynamic stability, as illustrated in Fig. 4 (a-d). Additionally, the total energy oscillation per atom around the equilibrium position remained within 0.025 eV, indicating outstanding thermal stability.

3.2. *Band alignment and charge separation efficiency*

In OWS, comprehending the dynamics of electrons and holes proximate to the junction is imperative for studying the processes of HER and OER, respectively. Additionally, the establishment of ΔCBO (conduction band offset) and ΔVBO (valence band offset) is pivotal. To address this, we conducted comprehensive calculations utilizing the HSE06 hybrid functional to determine the electrostatic potential and average electrostatic potential for both zigzag and armchair in-plane interfaces. Intriguingly, our analysis revealed the absence of band offset formation in the armchair interface, while distinctive band offsets were observed in the zigzag interface. Specifically, the calculated ΔCBO and ΔVBO for the zz-MoS_2/WS_2 in-plane interface are graphically presented in Fig. 5. The obtained values were respectively 0.91 eV and 0.71 eV for ΔCBO and ΔVBO. Notably, our findings suggest that electrons exhibit facile mobility from the conduction band of WS_2 to that of MoS_2, while holes readily migrate from the valence band of MoS_2 to that of WS_2. This

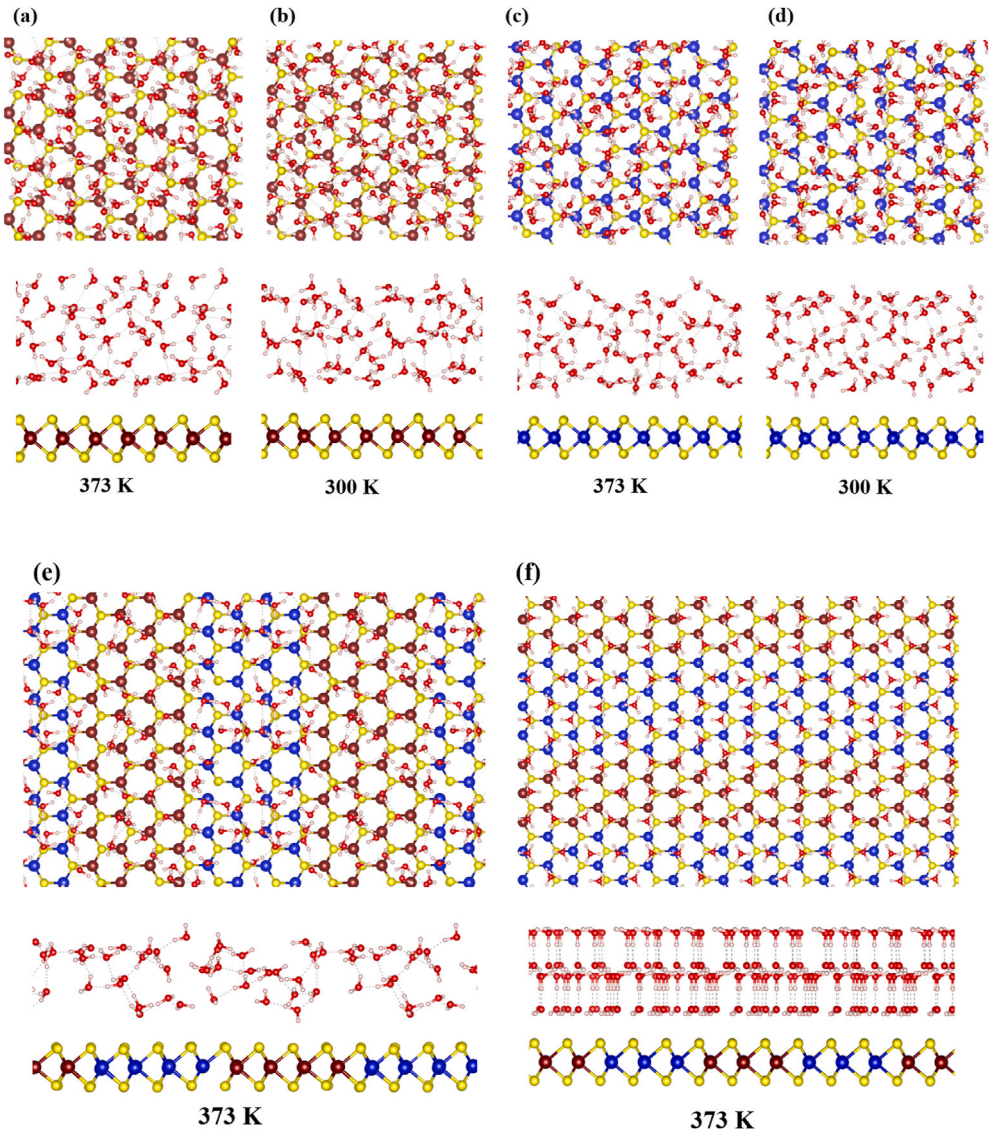

Fig. 3. AIMD simulation of water on the MoS_2, WS_2 monolayers and MoS_2/WS_2 in-plane interfaces at different temperatures. AIMD snapshots of different orientations of; (a–b) MoS_2 monolayer, (c–d) WS_2 monolayer, (e) Zigzag MoS_2/WS_2 interface, (f) Armchair MoS_2/WS_2 interface. The time for the MD simulation was set to 10 ps.

intriguing behavior leads to the holes and electrons at the opposite sides of the junction, culminating in the formation of substantial quantum wells. Motivated by these outcomes, we have selected the zigzag in-plane interface of MoS_2/WS_2 as the focal point for investigating catalytic activity, with a specific emphasis on understanding the HER at the MoS_2 and OER at the WS_2. This strategic choice aligns with our objective to unravel the nuanced interplay of charge carriers and band alignments within the heterostructure, contributing valuable insights to the catalytic mechanisms governing water splitting processes.

To qualitatively visualize the hole and electron separation and their transfer at the junction in zz-MoS_2/WS_2 in-plane heterostructure, we have calculated the charge distribution in the CBM (conduction band minimum) and VBM (valence band maximum) at the Gamma point of the Brillouin zone with an isosurface value of 1.95×10^{-7} e/ Å as well as the electronic differential charge density difference $(\Delta\rho = \rho_{MoS_2/WS_2} - \rho_{MoS_2} - \rho_{WS_2})$ as shown Fig. 6(a-c). The results shows that the conduction band minimum and valence band maximum is contributed from MoS_2 and WS_2 monolayers respectively, demonstrating a heterojunction of type-II alignment. The charge transfer mechanisms at the interface are also shown in Fig. 6(c). Furthermore, the type-II alignment also confirmed with the LDOS (local density of states) and projected orbital analysis. The LDOS, in Fig. 6(d), shows that the valence band maximum is from WS_2 monolayer and the conduction band is minimum from MoS_2 monolayer, respectively. This reflects further confirmation of the type-II alignment in the zz-MoS_2/WS_2 in-plane heterostructure. The projected electronic structures in Fig. 7 (a-d), shows that the alignment is due to the Mo-$d_{3z^2-r^2}$ and W-$d_{3z^2-r^2}$ orbitals.

3.3. Overall water splititng

The process of OWS involves generating oxygen and hydrogen through two distinct reactions: OER and HER [49]. The OER, in particular, presents a significant challenge, as it comprises a complex mechanism (four-steps) requiring four holes to produce one molecule of O_2 from two molecules of H_2O. Initially, a water molecule reacts with the active catalyst, leading to the formation of a H^+ (hydrogen ion) and an OH* species. Subsequently, the species (OH*) reacts with a hole, transforming to species (O*), while releasing a H^+. In step third, the O* species, in the presence of H_2O molecule, interacts with a hole to produce an O–H–O* species, simultaneously releasing a H^+. Finally, the

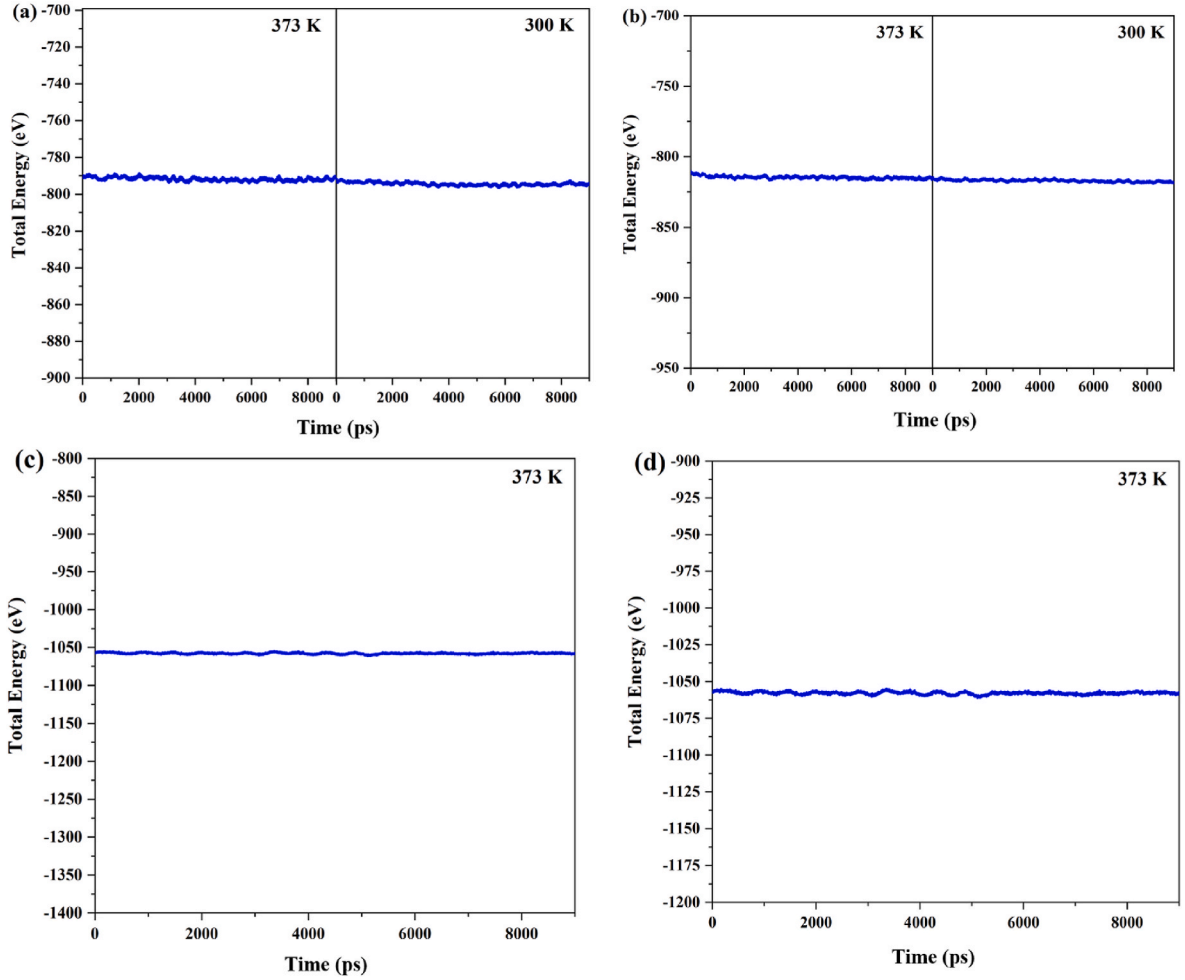

Fig. 4. Total energy fluctuations observed in the AIMD simulation at different temperatures; (a) MoS_2 monolayer, (b) WS_2 monolayer, (c) Zigzag MoS_2/WS_2 heterostructure, (d) Armchair MoS_2/WS_2 heterostructure. The time steps for the MD simulation were set to 10 ps.

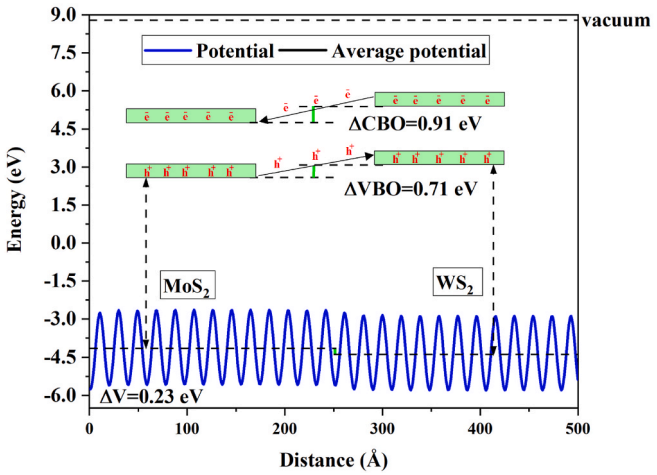

Fig. 5. Schematic representation of the ΔCBO and ΔVBO formation and electrons/holes flow for the zigzag MoS_2/WS_2 in-plane interface by potentials line up method. Where the blue wave shape represents the electrostatic potentials and the middle black line is the average electrostatic potentials. (For interpretation of the references to colour in this figure legend, the reader is referred to the Web version of this article.)

O–H–O* species, upon encountering a hole, generates O_2* and another H^+. However, O_2* is inherently unstable and promptly desorbs from the photocatalyst surface as an O_2 molecule. The entire process can be represented by the below chemical reactions (1)–(5).

$$H_2O_{(l)} + * + h^+ \rightarrow OH^* + H^+ \quad (1)$$

$$OH^* + h^+ \rightarrow O^* + H^+ \quad (2)$$

$$O^* + H_2O_{(l)} + h^+ \rightarrow O\text{–}H\text{–}O^* + H^+ \quad (3)$$

$$O\text{–}H\text{–}O^* + h^+ \rightarrow O_2^* + H^+ \quad (4)$$

$$O_2^* + h^+ \rightarrow * + O_{2(g)} \quad (5)$$

And the HER reaction is given below into two steps (6)–(7).

$$* + H^+ + e^- \rightarrow H^* \quad (6)$$

$$* + H^+ + e^- \rightarrow H_{2(g)} \quad (7)$$

In the equations above, the symbol * denotes the zigzag MoS_2-WS_2 in-plane heterostructure photocatalyst, while OH^*, O^*, $O\text{–}H\text{–}O^*$, O_2^*, and H^* represent the species, which exhibit high reactivity with the electrolyte. The ΔG (Gibbs free energy difference) value in eV, in equations (1)–(7) is calculated according to the Nørskov model [50]. At pH = 0, the formula is given as: $\Delta G = \Delta E + \Delta E_{zpe} - T\Delta S$, where ΔE represents the difference in adsorption energy, ΔS and ΔE_{zpe} denote the entropy difference and zero-point energy difference among the gas phases and adsorbed states, respectively. The ΔG value between the

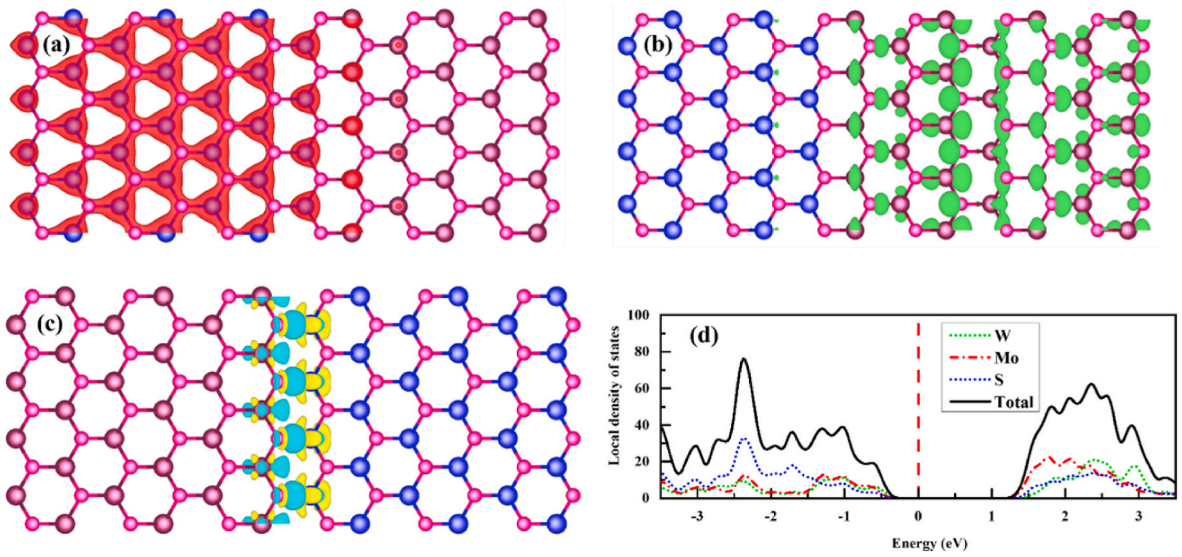

Fig. 6. The CBM and VBM for zz-MoS_2/WS_2 in-plane heterostructure; (a) VBM on WS_2 side (b) CBM on MoS_2 side (c) charge transfer at the junction (d) LDOS.

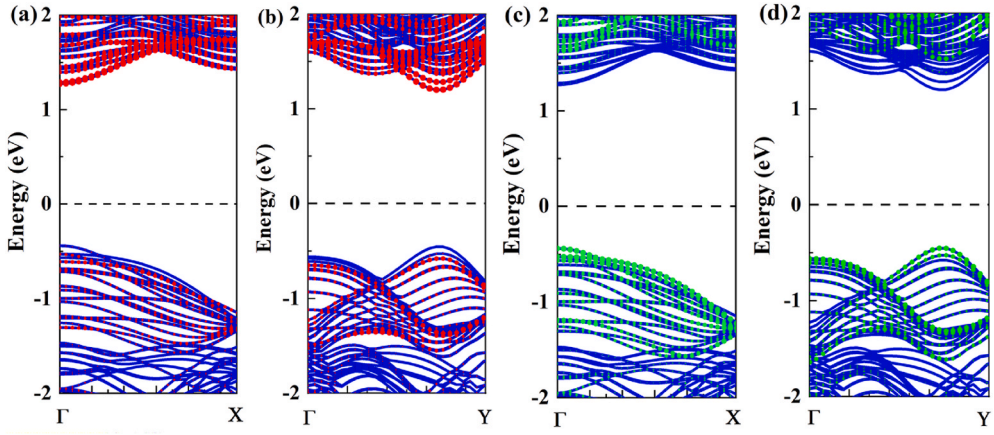

Fig. 7. The HSE06 calculated weighted bands of zz-MoS_2/WS_2 in-plane heterostructure for; (a–b) Mo-$d_{3z^2-r^2}$ orbitals and (c–d) W-$d_{3z^2-r^2}$ orbitals.

reactants and products in the above reactions are given below in equations (8)–(14).

$$\Delta G1 = G_{OH}^{*} + G_H^{+} - G_{H2O} - G(^{*}) - U_h \quad (8)$$

$$\Delta G2 = G_{O^{*}} + G_H^{+} - G_{OH}^{*} - U_h \quad (9)$$

$$\Delta G3 = G_{O\text{-}H\text{-}O}^{*} + G_H^{+} - G_O^{*} - G_{H2O} - U_h \quad (10)$$

$$\Delta G4 = G_{O2}^{*} + G_H^{+} - G_{O\text{-}H\text{-}O}^{*} - U_h \quad (11)$$

$$\Delta G5 = G(^{*}) + G_{O2} - G_{O2}^{*} - U_h \quad (12)$$

$$\Delta G6 = G_H^{*} - G(^{*}) - G_H^{+} - U_e \quad (13)$$

$$\Delta G7 = G_{H2} - G(H^{*}) - G_H^{+} - U_e \quad (14)$$

In the above equations, at room temperature and pressure, we exchanged the free energy of hydrogen ion with $\frac{1}{2}G_{H_2}$. The catalyst efficiency is defined by the reaction overpotential (η), which can be calculated as: $\eta_{OER} = \max[\Delta G_1, \Delta G_2, \Delta G_3, \Delta G_4, \Delta G_5]/e - 1.23$. In this formula the 1.23 V, represents the potential at room temperature and pressure that can split the water molecule into H_2 and O_2 [10]. And ΔG_1, ΔG_2, ΔG_3, ΔG_4 and ΔG_5, represents the free energy change in the reactions and *e* is the electron transfer. The OER calculated free energies for zz-MoS_2/WS_2 composite are given in Fig. 8(a). The calculated OER overpotentials for zz-MoS_2/WS_2 in-plane heterostructure at hole potential zero is 1.5 V. But when we employed the hole potentials, its value dropped to 0.96 V. The calculated ΔG (eV) of HER for zz-MoS_2/WS_2 in-plane heterostructure are shown in Fig. 8(b). In case of HER reactions, the ΔG (eV) values are about zero, which represents a candidate catalyst for HER [18,19]. The overpotentials for HER on the zz-MoS_2/WS_2 in-plane heterostructure is 0.32 V. This observation underscores the potential of zigzag MoS_2/WS_2 in-plane heterostructure as high efficiency bi-functional photocatalyst towards HER and OER activation.

3.4. The STH efficiency of H_2 conversion

The STH conversion efficiency of the zigzag MoS_2-WS_2 in-plane heterostructure was calculated with the reported model [51]. The model involved three parameters such as light absorption (η_{labs}) and carrier utilization (η_{cu}) and STH efficiency (η_{STH}) as following.

$$\eta_{STH} = \eta_{abs} \times \eta_{cu} \quad (15)$$

The light absorption efficiency is defining below;

$$\eta_{abs} = \frac{\int_{Eg}^{\infty} p(h\omega)d(h\omega)}{\int_{0}^{\infty} p(h\omega)d(h\omega)} \quad (16)$$

In the above function E_g and $p(h\omega)$ indicates the band gap of the

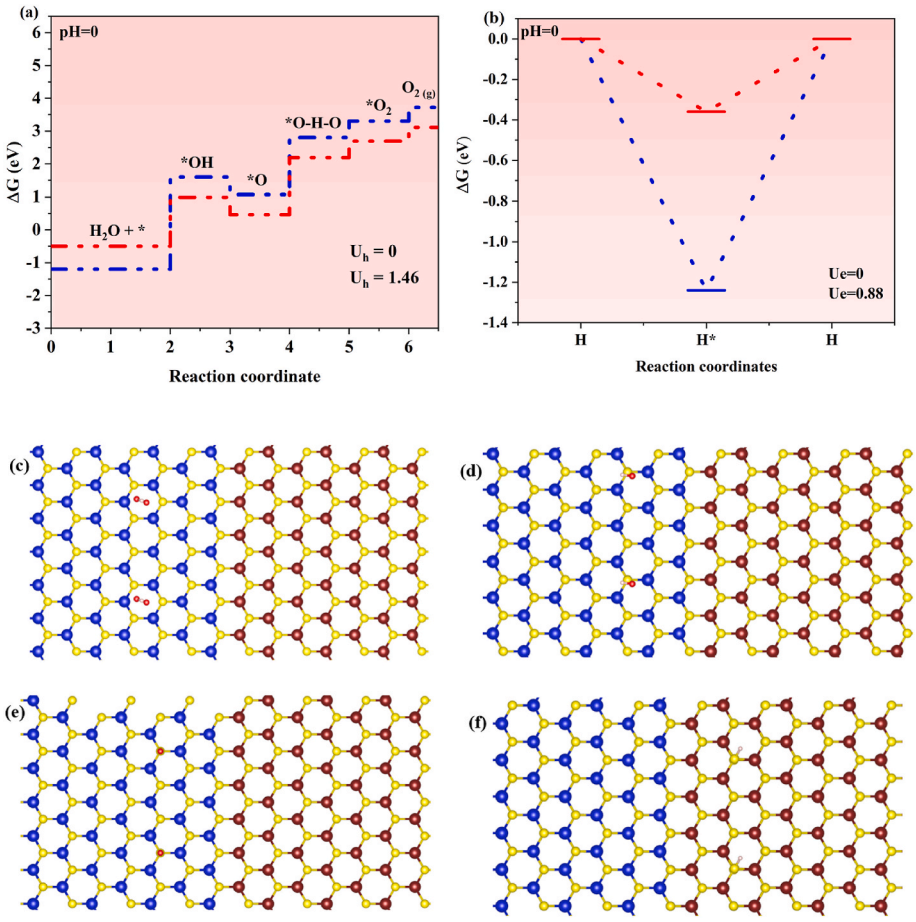

Fig. 8. The photocatalytic overall water splitting mechanisms on the zz-MoS_2/WS_2 in-plane interface; (a) OER (b) HER.

materials and sun flux at AM1.5G spectrum. The η_{cu} (carrier utilization efficiency) is given as;

$$\eta_{cu} = \frac{\Delta G \int_E^{\infty} \frac{p(h\omega)}{h\omega} d(h\omega)}{\int_{Eg}^{\infty} p(h\omega) d(h\omega)} \quad (17)$$

In this function the free energy for water splitting is given by (ΔG), which is 1.23 V [10]. And the incident photon energy is defined as;

$$E = \begin{cases} Eg, (\chi(H_2) \geq 0.2, (\chi(O_2) \geq 0.6) \\ Eg + 0.2 - \chi(H_2), (\chi(H_2) < 0.2, (\chi(O_2) \geq 0.6) \\ Eg + 0.6 - (\chi(O_2), \chi(H_2) \geq 0.2, (\chi(O_2) < 0.6) \\ Eg + 0.8 - \chi(H_2) - \chi(O_2), (\chi(H_2) < 0.2, (\chi(O_2) < 0.6) \end{cases}$$

By combining equations (16) and (17), the η_{STH} can be obtained as;

$$\eta_{STH} = \frac{\Delta G \int_E^{\infty} \frac{p(h\omega)}{h\omega} d(h\omega)}{\int_0^{\infty} p(h\omega) d(h\omega)} \quad (18)$$

The calculated STH efficiency of the zz-MoS_2/WS_2 in-plane heterostructure is 12.29%. The projected STH efficiency surpasses the necessary efficiency criterion (10%) for hydrogen conversion in commercial applications [52]. The high value of η_{STH}, make the zz-MoS_2/WS_2 in-plane heterostructure outstanding candidate for generation of hydrogen.

4. Conclusion

OWS represents an optimal method for directly converting solar energy into hydrogen fuel. However, the challenge persists in discovering a catalyst with both robust thermodynamic stability and favorable electronic properties. In this context, DFT and AIMD simulations were conducted to assess the interfacial properties and thermal stability of zigzag and armchair MoS_2/WS_2 in-plane heterostructures for OWS. AIMD simulations revealed that both the zigzag and armchair MoS_2/WS_2 in-plane heterostructures maintain thermodynamic stability under operational conditions. Nevertheless, the zigzag MoS_2/WS_2 in-plane heterostructure demonstrated superior charge separation efficiency and exhibited larger band offsets compared to its armchair counterpart. The distinctive chemical bonding and type-II band alignment at the zigzag interface significantly enhance charge transfer and separation within this heterostructure. This lateral heterostructure exhibits exceptional photocatalytic performance, with ultra-low overpotentials for OER (0.96 V) and HER (0.3 V) at pH = 0. Additionally, it boasts a high STH efficiency of 12.29%, positioning it as an excellent candidate for practical implementation in OWS applications. The insights from this research offer a pathway for further exploration of in-plane interface formation among diverse materials, thereby advancing OWS technology.

CRediT authorship contribution statement

Shafiq Ur Rehman: Writing – original draft, Software, Methodology, Investigation. **Qihui Sun:** Writing – review & editing, Data curation. **Junwei Wang:** Writing – review & editing. **Weiqiang Lv:** Writing – review & editing, Formal analysis, Data curation. **Azim Khan:** Writing – review & editing. **Yifan Liu:** Writing – review & editing, Validation, Conceptualization. **Nasir Mahmood:** Writing – review & editing, Supervision, Formal analysis, Conceptualization. **Jian Xian:** Writing – review & editing, Validation, Supervision, Funding acquisition, Formal analysis.

Declaration of competing interest

The authors declare the following financial interests/personal relationships which may be considered as potential competing interests:

Shafiq Ur Rehman reports financial support was provided by University of Electronic Science and Technology of China. Shafiq Ur Rehman reports a relationship with The University of North Carolina at Chapel Hill that includes:. If there are other authors, they declare that they have no known competing financial interests or personal relationships that could have appeared to influence the work reported in this paper.

Acknowledgements

The financial supported in this work was provided by National Natural Science Foundation of China (No. 51972045), the Fundamental Research Funds for the Chinese Central Universities, China (ZYGX2019J025), Sichuan Science and Technology Program (2022NSFSC1087, 2021YFG0373).

References

[1] Zhang P, Zhang J, Gong J. Tantalum-based semiconductors for solar water splitting. Chem Soc Rev 2014;43:4395–422.
[2] Gopinath CS, Nalajala N. A scalable and thin film approach for solar hydrogen generation: a review on enhanced photocatalytic water splitting. J Mater Chem A 2021;9:1353–71.
[3] Li R, Weng Y, Zhou X, Wang X, Mi Y, Chong R, Han H, Li C. Achieving overall water splitting using titanium dioxide-based photocatalysts of different phases. Energy Environ Sci 2015;8:2377–82.
[4] Yu J, Li Z, Wang C, Xu X, Liu T, Chen D, Shao Z, Ni M. Engineering advanced noble-metal-free electrocatalysts for energy-saving hydrogen production from alkaline water via urea electrolysis. J Colloid Interface Sci 2024;661:629–61.
[5] Rehman SU, Wang J, Wu G, Ali S, Xian J, Mahmood N. Unraveling the photocatalytic potential of transition metal sulfide and selenide monolayers for overall water splitting and photo-corrosion inhibition. J Mater Chem A 2024;12:6693–702.
[6] Wang Z, Li C, Domen K. Recent developments in heterogeneous photocatalysts for solar-driven overall water splitting. Chem Soc Rev 2019;48:2109–25.
[7] Kudo A, Miseki Y. Heterogeneous photocatalyst materials for water splitting. Chem Soc Rev 2009;38:253–78.
[8] Xu L, Zeng J, Li Q, Luo X, Chen T, Liu J, Wang LL. Multifunctional silicene/CeO_2 heterojunctions: desirable electronic material and promising water-splitting photocatalyst. Chin Chem Lett 2022;33:3947–50.
[9] Wu W, Jiang C, Roy VA. Recent progress in magnetic iron oxide–semiconductor composite nanomaterials as promising photocatalysts. Nanoscale 2015;7:38–58.
[10] Walter MG, Warren EL, McKone JR, Boettcher SW, Mi Q, Santori EA, Lewis NS. Solar water splitting cells. Chem Rev 2010;110:6446–73.
[11] Rao T, Wang H, Zeng YJ, Guo Z, Zhang H, Liao W. Phase transitions and water splitting applications of 2D transition metal dichalcogenides and metal phosphorous trichalcogenides. Adv Sci 2021;8:2002284. 19.
[12] Qorbani M, Sabbah A, Lai YR, Kholimatussadiah S, Quadir S, Huang CY, Shown I, Huang YF, Hayashi M, Chen KH. Atomistic insights into highly active reconstructed edges of monolayer 2H-WSe_2 photocatalyst. Nat Commun 2022;13:1256–7.
[13] Zhang W, Yin Y, He C. Spontaneous enhanced visible-light-driven photocatalytic water splitting on novel type-II GaSe/CN and Ga_2SSe/CN vdW heterostructures. J Phys Chem Lett 2021;12:5064–75.
[14] da Silva R, Barbosa R, Mancano RR, Duraes N, Pontes RB, Miwa R, Fazzio A, Padilha JE. Metal chalcogenides Janus monolayers for efficient hydrogen generation by photocatalytic water splitting. ACS Appl Nano Mater 2019;2:890–7.
[15] Rehman SU, Ding ZJ. Enhanced electronic and optical properties of three TMDCs monolayers. Phys Chem Chem Phys 2018;20:16604–14.
[16] Rehman SU, Amin B, Hafeez M, Khan SA, Mir IA, Uddin W, Wei L, Zhu L. Realization of noble heterobilayers with enhanced optoelectronic properties. Appl Surf Sci 2020;505:1445–9.
[17] Velpandian M, Ummethala G, Mallad SK, Meduri P. Heterostructures of tin and tungsten selenides for robust overall water splitting. J Colloid Interface Sci 2022;623:561–73.
[18] Mondal A, Vomiero A. 2D transition metal dichalcogenides-based electrocatalysts for hydrogen evolution reaction. Adv Funct Mater 2022;32:2208994. 28.
[19] Jing Y, Zhou Z, Geng W, Zhu X, Heine T. 2D honeycomb-kagome polymer tandem as effective metal-free photocatalysts for water splitting. Adv Mater 2021;33:2008645–8.
[20] Chandrasekaran S, Yao L, Deng L, Bowen C, Zhang Y, Chen S, Lin Z, Peng F, Zhang P. Recent advances in metal sulfides: from controlled fabrication to electrocatalytic, photocatalytic and photoelectrochemical water splitting and beyond. Chem Soc Rev 2019;48:4178–280.
[21] Fu CF, Li X, Yang J. A rationally designed two-dimensional $MoSe_2/Ti_2CO_2$ heterojunction for photocatalytic overall water splitting: simultaneously suppressing electron–hole recombination and photo-corrosion. Chem Sci 2021;12:2863–9.
[22] Li S, Xu W, Meng L, Tian W, Li L. Recent progress on semiconductor heterojunction-based photoanodes for photoelectrochemical water splitting. Small Sci 2022;2:2100112–23.
[23] Li J, Yuan H, Zhang W, Jin |B, Feng Q, Huang J, Jiao Z. Advances in Z-scheme semiconductor photocatalysts for the photoelectrochemical applications: a review. Carbon Energy 2022;4:294–331.
[24] Li L, Yang H, Yang P. $WS_2/MoSe_2$ van der Waals heterojunctions applied to photocatalysts for overall water splitting. J Colloid Interface Sci 2023;650:1312–8.
[25] Yang R, Fan Y, Zhang Y, Mei L, Zhu R, Qin J, Hu J, Chen Z, Ng YH, Voiry D, Li S, Lu Q, Wang Q, Yu JC, Zeng Z. 2D transition metal dichalcogenides for photocatalysis. Angew Chem Int Ed 2023;62:2022180. 29.
[26] Sulas-Kern DB, Miller EM, Blackburn JL. Photoinduced charge transfer in transition metal dichalcogenide heterojunctions–towards next generation energy technologies. Energy Environ Sci 2020;13:2684–740.
[27] Fu CF, Zhang R, Luo Q, Li X, Yang J. Construction of direct Z-Scheme photocatalysts for overall water splitting using two-dimensional van der Waals heterojunctions of metal dichalcogenides. J Comput Chem 2019;40:980–7.
[28] Qiang Z, Zhang Y, Ding JX, Xie KX, Nouguiza H, Chen HX, Duan L, Fan JB, Ni L. Design of a direct Z-scheme GeC/arsenene van der Waals heterostructure as highly efficient photocatalysts for water splitting. Int J Hydrogen Energy 2024;51:809–21.
[29] Kim MS, Don WJ, Hong S, Ri M, Yang S. Photocatalytic property of two dimensional heterostructure MoS_2/WS_2 for hydrogen evolution via water splitting: a first principles calculation. Int J Hydrogen Energy 2023;48:9371–6.
[30] Liu Y, Sun J, Zhou X, Lv C, Zhou Y, Cong B, Chen G. An in-plane S-scheme heterostructure drives H_2 production with water and solar energy. J Chem Eng 2022;437:135280. 11.
[31] Ge C, Wang B, Yang H, Feng Q, Huang S, Zu X, Li L, Deng H. Direct Z-scheme GaSe/ZrS_2 heterojunction for overall water splitting. Int J Hydrogen Energy 2023;48:13460–9.
[32] Li H, Xu L, Huang X, Yang JO, Chen M, Zhang Y, Tang S, Dong K, Wang LL. Two-dimensional C_3N/WS_2 vdW heterojunction for direct Z-scheme photocatalytic overall water splitting. Int J Hydrogen Energy 2023;48:2186–99.
[33] Qian G, Liu Y, Huang S, Dai S, Wang Y, Luo X, Xie Q. Efficient interfacial charge transfer in the $MoSe_2$/SPtSe heterostructure improves the efficiency of hydrogen production from water splitting: a S-scheme photocatalyst. Int J Hydrogen Energy 2024;66:676–88.
[34] Rosati R, Paradisanos I, Huang L, Gan Z, George A, Watanabe K, Taniguchi T, Lombez L, Renucci P, Turchanin A. Interface engineering of charge-transfer excitons in 2D lateral heterostructures. Nat Commun 2023;14:2438. 8.
[35] Zhou Y, Zhang J, Song E, Lin J, Zhou J, Suenaga K, Zhou W, Liu Z, Liu J, Lou J. Enhanced performance of in-plane transition metal dichalcogenides monolayers by configuring local atomic structures. Nat Commun 2020;11:2253–9.
[36] Tang Y, Liu M, Zhong X, Qiu K, Bai L, Ma B, Wang J, Chen Y. Theoretical design of Sc_2CF_2/Ti_2CO_2 heterostructure as a promising direct Z-scheme photocatalyst towards efficient water splitting. Results Phys 2024;60:107706–11.
[37] Wang J, Li Z, Chen H, Deng G, Niu X. Recent advances in 2D lateral heterostructures. Nano-Micro Lett 2019;11:1–31.
[38] Duan X, Wang C, Shaw JC, Cheng R, Chen Y, Li H, Wu X, Tang Y, Zhang Q, Pan A. Lateral epitaxial growth of two-dimensional layered semiconductor heterojunctions. Nat Nanotechnol 2014;9:1024–30.
[39] Lai G, Lyu LM, Huang YS, Lee GC, Lu MP, Perng TP, Lu MY, Chen LJ. Few-layer WS_2–MoS_2 in-plane heterostructures for efficient photocatalytic hydrogen evolution. Nano Energy 2021;81:105608. 8.
[40] Che W, Cheng W, Yao T, Tang F, Liu W, Su H, Huang Y, Liu Q, Liu J, Hu F, Pan Z, Sun Z, Wei S. Fast photoelectron transfer in C/C_3N_4 plane heterostructural nanosheets for overall water splitting. J Am Chem Soc 2017;139:3021–6.
[41] Cheng Z, Xiao Y, Wu W, Zhang X, Fu Q, Zhao Y, Qu L. All-pH-Tolerant in-plane heterostructures for efficient hydrogen evolution reaction. ACS Nano 2021;15:11417–27.
[42] Lu B, Zheng X, Li Z. Two-dimensional lateral heterostructures of triphosphides: AlP_3−GaP_3 as a promising photocatalyst for water splitting. ACS Appl Mater Interfaces 2020;12:53731–8.
[43] Kresse G, Furthmüller J. Efficient iterative schemes for ab initio total-energy calculations using a plane-wave basis set. Phys Rev B 1996;54:11169. 5.
[44] Perdew JP, Burke K, Ernzerhof M. Generalized gradient approximation made simple. Phys Rev Lett 1996;77:3865–8.
[45] Monkhorst HJ, Pack JD. Special points for Brillouin-zone integrations. Phys Rev B 1976;13:5188. 8.
[46] Grimme S. Accurate description of van der Waals complexes by density functional theory including empirical corrections. J Comput Chem 2004;25:1463–73.
[47] Mathew K, Sundararaman R, Weaver KL. Implicit solvation model for density-functional study of nanocrystal surfaces and reaction pathways. J Chem Phys 2014;140:084106. 6.
[48] Lv R, Robinson JA, Schaak RE, Sun D, Sun Y, Mallouk TE, Terrones M. Transition metal dichalcogenides and beyond: synthesis, properties and applications of single- and few-layer nanosheets. Acc Chem Res 2015;48:56–64.
[49] Chen S, Takata T, Domen K. Particulate photocatalysts for overall water splitting. Nat Rev Mater 2017;2:1–17.

[50] Nørskov JK, Rossmeisl J, Logadottir A, Lindqvist L, Kitchin JR, Bligaard T, Jonsson H. Origin of the overpotential for oxygen reduction at a fuel-cell cathode. J Phys Chem B 2004;108:17886–92.

[51] Fu CF, Sun J, Luo Q, Li X, Hu W, Yang J. Intrinsic electric fields in two-dimensional materials boost the solar-to-hydrogen efficiency for photocatalytic water splitting. Nano Lett 2018;18:6312–7.

[52] Cox CR, Lee JZ, Nocera DG, Buonassisi T. Ten-percent solar-to-fuel conversion with nonprecious materials. Proc Natl Acad Sci USA 2014;111:14057–61.